Optimisation of the Sorption of Selected Polycyclic Aromatic Hydrocarbons by Regenerable Graphene Wool

Adedapo O. Adeola [a] and Patricia B.C. Forbes [a*]

[a]*Department of Chemistry, Faculty of Natural and Agricultural Sciences, University of Pretoria, Lynnwood Road, Hatfield, Pretoria 0002, South Africa*.

Abstract

A novel graphene wool (GW) material was used as adsorbent for the removal of phenanthrene (PHEN) and pyrene (PYR) from aqueous solution. Adsorption kinetics, adsorption isotherms, thermodynamics of adsorption and effect of pH, ionic strength, and temperature on the adsorption of PHEN and PYR onto GW were comprehensively investigated. Isothermal and kinetic experimental data were fit to Langmuir, Freundlich, Temkin, Sips and Dubinin-Radushkevish (D-R) models, as well as pseudo-first-order and pseudo-second-order kinetic models. The adsorption kinetic data best fit the pseudo-second-order kinetic model for PHEN and PYR sorption with R^2 value >0.999, whilst the Sips model best fit isotherm data. Kinetic data revealed that 24 h of contact between adsorbent and PAHs was sufficient for maximum adsorption, where the Langmuir maximum adsorption capacity of GW for PHEN and PYR was 5 and 20 mg g^{-1} and the optimum removal efficiency was 99.9% and 99.1%, respectively. Thermodynamic experiments revealed that adsorption processes were endothermic and spontaneous. Desorption experiments indicated that irreversible sorption occurred with a hysteresis index greater that zero for both PAHs. The high adsorption capacity and potential reusability of GW makes it a very attractive material for removal of hydrophobic organic micro-pollutants from water.

Keywords: Adsorption; Graphene wool; Phenanthrene; Pyrene; Water treatment.

1.0. Introduction

Polycyclic aromatic hydrocarbons (PAHs) such as phenanthrene and pyrene are semi-volatile and hydrophobic organic pollutants, found ubiquitously in the environment. PAHs are directly released into the environment via effluent discharge from petroleum and petrochemical industries, subsurface fuel pipeline leakages, and continuous leakage of gasoline from underground storage tanks (Torabian *et al.* 2010; Abdel-Shafy & Kamel 2016). In addition, PAH contamination also arises from tobacco smoking, improper waste disposal and burning of biomass and organic substances (IARC 2010). Some PAHs are difficult to degrade, are carcinogenic or mutagenic and 16 PAHs are classified as priority pollutants by the United States Environmental Protection Agency (US EPA) (Cai *et al.* 2009). Upon human exposure, they permeate the cell membrane and are absorbed easily because they are carbon-rich and hydrophobic in nature (Yakout & Daifullah 2013).

The adsorption process has been identified as a suitable, simple and effective remediation approach for the removal of several pollutants from water without chemical transformation. Carbonaceous or carbon-based materials have been reported to be effective for the removal of PAHs, however, most of the adsorbents present several challenges including difficulties regarding regeneration and reusability of spent adsorbent (Wang *et al.* 2006; Yang & Xing 2007; Zhao *et al.* 2011; Yang *et al.* 2013; Yang *et al.* 2015; Hassan *et al.* 2018). The presence of carbonaceous materials in water bodies may influence the mobility and fate of organic pollutants, thereby influencing their environmental impact or risks (Liu *et al.* 2016). The adsorption of PAHs has been reported to have higher binding strength onto porous carbon than onto soils, suspended organic matter, and sediments (Ukalska-Jaruga *et al.* 2019). Therefore, a comprehensive understanding of the adsorption mechanism of organic contaminants onto graphene based materials will assist in

shedding light on the fate and distribution of PAHs in aquatic environments, and may provide the possibility of developing a novel adsorbent for water treatment applications. The graphene wool used in this study is a novel material synthesized via the chemical vapour deposition method onto a quartz wool substrate under optimized flow rates of hydrogen, argon and methane gas precursors (Schoonraad *et al.* 2020). This wool-like graphene material has not been applied to the removal of any class of pollutants in water to date. Despite several reports on adsorption of PAHs by different graphene based materials, information on the role of certain environmental variables such as total dissolved solids/salinity/ionic strength as well as thermodynamics of adsorption are unavailable or scanty. This study evaluates adsorption data for wide range of PAH concentrations (part-per-million and part-per-trillion), which has never been done for any adsorbent, bearing in mind that PAH concentrations in surface waters may differ for different geographical locations.

The overall goal of this work was to apply a novel, regenerable graphene wool material for the removal of phenanthrene and pyrene from water. The role of environmental or process variables such as pH, temperature, ionic strength/TDS of the solution and initial concentration of PAHs on the sorptive removal of the compounds was studied to establish the optimum conditions for effective use of graphene wool for water treatment applications.

2.0. Experimental methods

2.1. Synthesis of graphene wool (GW)

The procedure as reported in (Schoonraad *et al.* 2020) was used to prepare the GW. Briefly, quartz wool (Arcos Organics, New Jersey, USA) was placed in the middle of a horizontal quartz tube (50 mm o.d., 44 mm i.d., x 1000 mm length) in a OTF-1200X-50-5L high-temperature furnace (MTI Corporation, California, USA). A mixture of 500 sccm argon and hydrogen (both 99.999%, Afrox,

South Africa) was introduced into the system after which the temperature was ramped to 1200 °C. The substrate was annealed under these conditions for 10 min after which methane (99.95%, Afrox, South Africa) was introduced for graphene growth. After the growth period had elapsed, the system was cooled under Ar and H_2. Thermal reduction of the hydrocarbon precursor and graphene deposition on silicon substrate is a bottom-up or "growth" synthesis approach, therefore, it was not necessary to remove the substrate, thus the term 'graphene wool (GW)' in this study infers graphene coated on quartz wool.

2.2. Characterization of graphene wool adsorbent

The morphology and structure of graphene wool was characterized by a combination of techniques including Raman spectroscopy (WITec alpha300 RAS^+ confocal Raman microscope, WiTec, Germany) using a 532 nm excitation laser at low power (5 mW). XPS (K-Alpha, Thermo Fisher Scientific Inc., USA) was also used to characterise the sample composition, and the binding energies were referenced to the C 1s line at 284.8 eV. The analysis was carried out under ultra-high vacuum chamber using an Al Ka X-rays at 1486.66 eV, and a take-off angle of 20˚ was selected for higher surface sensitivity. Scanning electron microscopy (SEM) images were also taken using a Zeiss Ultra-Plus 55 field emission scanning electron microscope (FE-SEM), operated at 2.0 kV, Zeiss, Germany. High resolution transmission electron microscopy (TEM) images of graphene wool were taken using a JEOL JEM 2100F (JOEL Ltd, Tokyo, Japan) operated at 200 kV (Schoonraad *et al.* 2020). The specific surface area (SSA) of GW was carried out using modified Sears' method (Sears 1956).

2.3. Adsorption kinetics and isotherm experiments

Batch adsorption experiments of PAHs onto graphene wool (GW) were performed in 40 mL PTFE screw cap amber vials (Stargate Scientific, South Africa) sealed with aluminum foil at 25 ± 1 °C. Background solution (pH = 7.0) contained 0.01 mol/L $CaCl_2$ (ACE, South Africa) in deionized water with 200 mg/L NaN_3 (Sigma-Aldrich, Germany) as a biocide. The sorption kinetic studies were conducted for 48 hours with initial pyrene and phenanthrene concentrations of 50 ng/L (neat standards were purchased from Supelco, USA), and the solid-to-water ratio for graphene wool was 50 mg per 100 mL. Afterwards, the isotherm experiment was conducted with initial concentrations of the PAH solutions ranging from 300 ng/L to 800 ng/L and 1 mg/L to 5mg/L respectively. Adsorption isotherms of PHEN and PYR were also determined at varying temperatures of 35, 45 and 55 °C using a thermostated shaking water bath (Wisebath, Celsius Scientific, South Africa) to determine whether the adsorption process is exothermic or endothermic. The role of ionic strength on adsorption of PHEN and PYR onto GW was studied. The sorbates were prepared in 0.01, 0.1 and 1 M $NaCl_2$ (Merck, South Africa) and isotherms were determined. The solution pH was adjusted with 0.1 M HCl (Merck, South Africa) or NaOH (ACE, South Africa) over the pH range from 2 to 12, to study the influence of pH on the removal of PHEN and PYR from aqueous solutions. All the solutions were prepared using ultra-pure water obtained from a Milli-Q water purification system (Millipore, Bedford, MA, USA).

2.4. Quantification

After equilibration, the vials were centrifuged at 3000 rpm for 5 min to obtain a clear supernatant. The PAH concentrations in the supernatants were analyzed in triplicate (n=3) by fluorescence spectroscopy (Horiba Jobin Yvon Fluoromax-4 spectrofluorometer; excitation wavelength was 290 nm for PHEN and 300 nm for PYR). The regression coefficients (R^2) of matrix-matched

calibration curves were obtained from stock solutions of each PAH. The working solutions were in the range of 50 – 1000 ng/L and 1 – 5 mg/L for PHEN and PYR respectively. The equation of the curve was used to deduce the equilibrium concentration C_e. The amount of each solute adsorbed (q_e, mg/g) was calculated using the following mass-balance equation:

$$q_e = \frac{(C_0 - C_e)V_0}{S_m} \quad (1)$$

Where C_o (mg/L) is the initial concentration, C_e (mg/L) is the equilibrium solute concentration, V_o is the initial volume (L) and S_m is the mass (g) of the adsorbent.

$$\text{Removal efficiency (\%)} = \frac{(C_0 - C_e)}{C_0} \times 100 \quad (2)$$

Regeneration of the adsorbent and reusability tests were carried out by solid phase extraction using 10 mL hexane (≥97% HPLC grade, Sigma-Aldrich, Germany) and placed on the thermostatic shaker for 2 hours at room temperature. PAHs desorbed were quantified using GC-MS due to the expected low concentration (refer to Supplementary Information for details). Afterwards, the GW was dried in a muffle furnace (Labotec, South Africa) at a temperature of 70 ˚C for 4 hours and was allowed to cool before re-use.

3.0. Results and Discussion

3.1. Characterization of graphene wool (GW)

The pH of GW was found to be 6.1 and 7.1 in $CaCl_{2(aq)}$ solution and de-ionized water, respectively. The surface area of GW as determined using Sear's method is 279 m^2/g, lower than the theoretical surface area of graphene (2630 m^2/g), due to coverage over the quartz wool which ultimately defines the surface area (Stoller *et al.* 2008; Wang *et al.* 2014). Raman spectroscopy revealed a crystallite grain size of an average value of 24 nm with three prominent peaks at 1349, 1582 and

2630 cm^{-1} (Figure S1), which correspond to D, G and 2D bands caused by stretching vibrations of sp3 and sp2 carbon atoms, respectively (Wang *et al.* 2014; Ndiaye *et al.* 2018). XPS spectrum of graphene wool revealed the strongest peak of C=C at 284.4 eV which represent graphene and suggests that the D peak in the Raman spectrum is due to thermal disintegration of sp2 carbon network into nano-sized oxidized domains which occurred during CVD synthesis (Figure S1) (Chen *et al.* 2008; Schoonraad *et al.* 2020). SEM and TEM images (Figure S1) revealed varying translucence as a result of multiple layer staking of the graphene flake-like sheets. The presence of interstitial spaces was also confirmed within the GW aggregates (Figure S1). This suggest that adsorption of PHEN and PYR may occur via multilayer or monolayer coverage of the adsorbent, and/or pore filling mechanisms due to the layered-morphology of GW. The interstitial spaces within GW may also be available for adsorption of PAHs.

3.2. Adsorption kinetics

The pseudo-first-order and pseudo-second-order kinetic models were investigated and compared in order to study the mechanism of the adsorption process (Zhao *et al.* 2011). The kinetic parameters and correlation coefficients obtained from different models are summarized in Table 1. The kinetic model plots are shown in Figure 1.

Table 1: Coefficients of sorption kinetics for phenanthrene and pyrene removal by graphene wool (GW) adsorbent and their correlation coefficients (R^2) (Experimental conditions: C_o = 50 ng L^{-1}; dosage = 50 mg per 100 mL; mixing rate = 200rpm; T = 25 ± 1 °C; pH = 6.8 ± 0.2 for phenanthrene and pH = 6.7 ± 0.2 for pyrene).

Adsorption Kinetics	**Parameters**	**PAHs**	
		Phenanthrene	**Pyrenes**
First Order	*Calculated* $q_{e\ (mg\ g^{-1})}$	6.02	10.83
	Experiment $q_{e\ (mg\ g^{-1})}$	28.60	41.87
	$K_1\ (hr^{-1})$	0.0617	0.0774
	R^2	0.4227	0.5772
Second Order	*Calculated* $q_e\ (mg\ g^{-1})$	28.33	41.84
	Experiment $q_e\ (mg\ g^{-1})$	28.60	41.87
	$K_2\ (mg\ g^{-1}\ hr^{-1})$	0.0859	0.0410
	$h\ (mg\ g^{-1}\ hr^{-1})$	68.94	71.77
	R^2	0.9998	0.9995

The kinetic experimental data was a far better fit with the pseudo-second-order equation with a correlation coefficient (R^2) > 0.999, compared with the first-order model (Table 1). The steepness observed in the first 6 h of phenanthrene sorption and 10 h of pyrene sorption is attributed to fast initial sorption, due to easily accessible GW sorption sites available to the respective PAH, before a period of slower adsorption (Figure 1). On the basis of correlation coefficients (Zhao *et al*. 2011), the adsorption of PHEN and PYR by GW follows a second-order reaction pathway. The kinetic pathway established for the adsorption of PHEN and PYR onto GW is in agreement with kinetic

studies previously reported for reduced graphene oxide (RGO) adsorption of bisphenol-A, which followed second order adsorption kinetics (Xu *et al.* 2012). This further confirms that graphene based materials are efficient adsorbents of hydrophobic organic pollutants with high adsorption capacity. The experimental adsorption capacity q_e for GW adsorption of PHEN and PYR is 28.60 ng/g and 41.87 ng/g, which is similar to that which was predicted using the pseudo-second-order kinetic equation (28.33 and 41.84 ng/g respectively), which suggests that the adsorption process involves chemisorption (Yu *et al.* 2015).

PHEN and PYR do not contain functional groups which would undergo chemical reactions with GW, but rather chemical interaction involving electron sharing and/or exchange between these PAHs and GW can be expected (Martínez *et al.* 2006). The adsorption rate constant k_2 for adsorption of phenanthrene and pyrene by GW is 0.0859 ng $g^{-1}hr^{-1}$ and 0.0410 ng g^{-1} hr^{-1}, and given that the second order pathway best describes the sorption process, it can be inferred that the smaller phenanthrene molecule is adsorbed at a faster rate than pyrene.

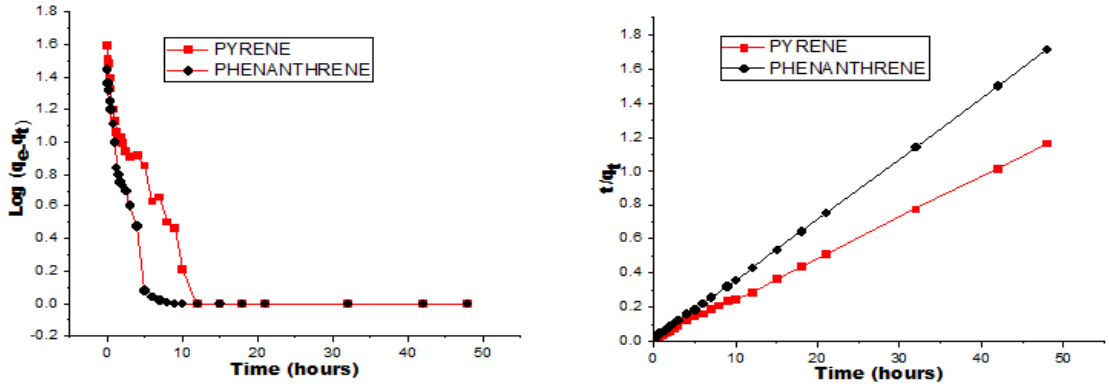

Figure 1*: Lagergren pseudo-first-order and pseudo-second-order kinetics sorption for pyrene and phenanthrene onto graphene wool (Experimental conditions: C_o = 50 ng $L^{-}1$; dosage = 50 mg per 100 mL, mixing rate = 200 rpm, T = 25 ± 1 °C; pH (PYR) = 6.7 ± 0.2 and pH (PHEN)= 6.8 ± 0.2).*

3.3. Sorption isotherm experiments

3.3.1. Effect of initial concentrations

Adsorption isotherm models are used to elucidate the sorbent-sorbate interactions when the adsorption process reaches equilibrium (Zhang *et al.* 2014). The adsorption isotherms of pyrene and phenanthrene on graphene wool are shown in Figure 3. The role of two different ranges of concentrations (with difference in magnitude of 10^{-6} g/L solute concentration) was used to explain the interaction between PAHs and GW and how concentration could affect the nature of adsorption. The isotherm regression plots and parameters for Freundlich, Langmuir, Temkin, Sips and Dubinin-Radushkevish models are presented in Table 2 and Figure 2 for concentrations in the part-per-million (mg/L) range and Table S2 and Figure S2 for concentrations in the part-per-trillion (ng/L) range. The correlation coefficient revealed that the isotherm models fit better with equilibrium data in the high concentration (mg/L) range, with R^2 values ranging from 0.9414 to 0.9984 than at lower concentration range (ng/L) with R^2 ranging from 0.7441 to 0.9928 (Table 3 and S2).

The Sips isotherm model best fit the data for PHEN and PYR sorption onto GW at high concentration range with R^2 and N values of (0.9956, 0.46) and (0.9984, 0.54) respectively, which suggests that a multilayer adsorption pattern on a heterogeneous surface is likely to define the sorption process of PHEN and PYR rather than the monolayer adsorption mechanism postulated by Langmuir (Allen *et al.* 2004). Comparatively, the equilibrium data for the low concentration range (ng/L) fit best the Temkin isotherm model with an R^2 value of 0.9443 for PHEN and 0.9928 for PYR sorption, which explains that the decline in heat of sorption with increase in adsorption coverage area is linear rather than logarithmic, as the Freundlich equation implies (Vidal *et al.* 2011). The mean sorption energy (E) for PHEN and PYR in the D-R model and high values of the

Temkin isotherm constant b_T suggests that interactions exist between GW and the PAHs, which is characteristic of electron transfer and/or sharing leading to $\pi - \pi$ interactions (Wang *et al.* 2014).

The Freundlich and Sips constant "*N*" indicates the heterogeneity index of the surface of the adsorbent and adsorption intensity due to the formation of new adsorption sites and increase in the adsorption capacity. This explains why the Langmuir maximum adsorption capacity is higher for PYR (20 mg/g) with *N* value of 0.9665 and 0.54 for Freundlich and Sips respectively, when compared with values obtained for PHEN (5 mg/g) (Table 3). This can be attributed to the physicochemical properties of compounds (Table S1) such as hydrophobicity (Log *Kow*), relative solubility (PYR: 0.135 mg/L, PHEN: 1.18 mg/L @ 25ºC) and the stronger π-π interactions as a result of the higher number of delocalized electrons, are all possible explanation to why PYR has greater maximum adsorption capacity onto GW than PHEN (Zhang *et al.* 2014).

Pyrene and phenanthrene, as well as other PAHs, possess high octanol-water partition coefficients LogK_{ow} (PYR 5.18 and PHEN 4.57) (Yakout & Daifullah 2013) and are very likely to be adsorbed onto hydrophobic surfaces (Khan *et al.* 2007). The maximum adsorption capacity q_{max} for Langmuir and Sips at lower concentration deviated from what was found for PAHs at high concentration (Table 2 and Table S2). At lower concentrations, the lower molecular weight compound (PHEN 178 g mol^{-1}) was better adsorbed onto GW than the higher molecular weight compound (PYR 202.25 g mol^{-1}) via a pore-filling mechanism on porous materials as described by the D-R model with equally strong correlation values of 0.9684 and 0.8770 for PYR and PHEN sorption (Table S2). This is in accordance with Wang et al. (2006), in that the molecular size of compounds in relation with pore size of adsorbent is one of the important factors that may influence sorption. The Langmuir dimensionless constant R_L, which indicates how favourable adsorption is, was less than 1 (Table 2 and S2), which indicates favourable adsorption of the selected PAHs onto

GW at both mg/L and ng/L concentration ranges (Rahman & Islam 2009). The linear relationship between LogK_{ow} and adsorption capacity was also reported by Khan et al. (2007) for PAH adsorption by different adsorbents. However, it is worthy to mention that GW has a much higher adsorption capacity within the same concentration range for PHEN sorption with a K_f value of 16.2 $mg^{1-1/n} L^{1/n} g^{-1}$, higher than polyester fiber, kapok and cattail adsorbents used in the respective studies, with K_f values of 2.15, 1.95 and 5.14 $mg^{1-1/n} L^{1/n} g^{-1}$ respectively (Khan *et al.* 2007).

In summary, adsorption of phenanthrene and pyrene increased with increase in initial PAH concentration and the positive correlation of high initial PAH concentrations with adsorption capacity of GW can be attributed to the larger number of PAH molecules available for interaction with active sites of the GW.

Table 2*:* Coefficents obtained for four different sorption isotherm models for phenanthrene and pyrene adsorption by graphene wool (GW) and their correlation coefficients (R^2) in the part-per-million PAH concentration ranges (Experimental conditions: Dosage = 20 mg per 30 mL; mixing rate = 220 rpm; T = 25 ± 1 °C; initial conc.: 1-5 mg/L; contact time = 24 hours; pH = 6.8 ± 0.2 for phenanthrene and pH = 6.7± 0.2 for pyrene).

Isotherm model	**Parameter**	**PAH**	
		Phenanthrene	**Pyrene**
Dubinin-Radushkevish	$Q_D\ (mol\ g^{-1})$	1.0053	1.0008
	$B_D\ (Kj\ mol^{-1}\ K^{-1})$	6.05×10^{-8}	1.01×10^{-8}
	$E\ (Kj\ mol^{-1})$	2.87	7.04
	R^2	0.9812	0.9920
Freundlich	N	0.6218	0.9665
	$K_f\ (mg^{1-1/n}\ L^{1/n}\ g^{-1})$	16.2	114.4
	R^2	0.9906	0.9685
Langmuir	$q_{max}\ (mg\ g^{-1})$	5.0	20.0
	$K_L\ (L\ mg^{-1})$	181.8	6.85
	R_L	0.0055	0.127
	R^2	0.9793	0.9635
Sips *(Freundlich-Langmuir)*	$q_{max}\ (mg\ g^{-1})$	5×10^{7}	1.43×10^{8}
	$K_s\ (L\ mg^{-1})$	7.7×10^{-8}	1.1×10^{-7}
	N	0.46	0.54
	R^2	0.9956	0.9984
Temkin	$b_T\ (Kj\ mol^{-1})$	15.4	22.3
	$K_T\ (L\ mg^{-1})$	6.87×10^{18}	1.51×10^{15}
	R^2	0.9414	0.9872

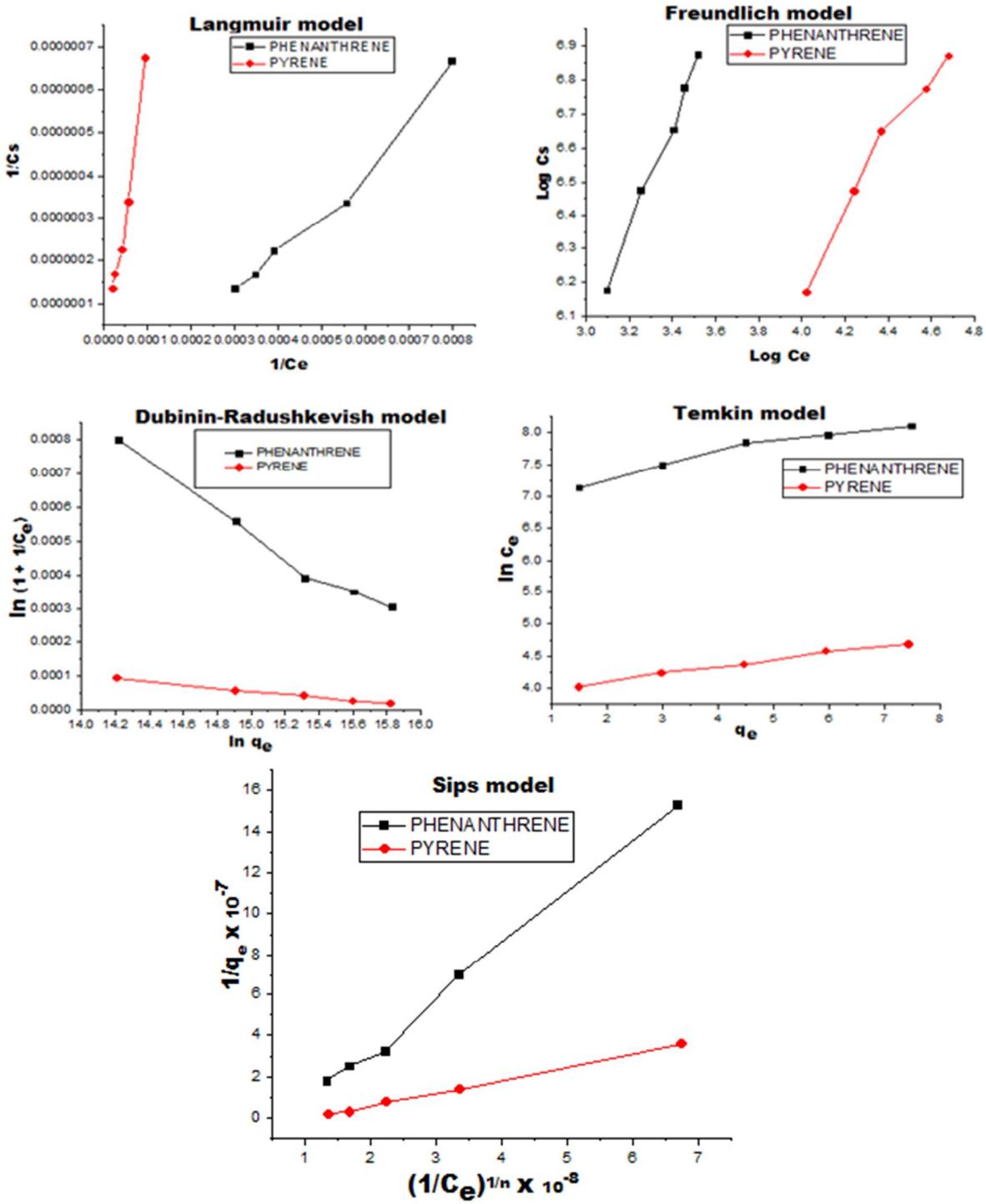

ion

Figure 2: *Plots of isotherm models fit to experimental data for phenanthrene and pyrene adsorption onto graphene wool*

3.3.2. Effect of contact time

Figure S3 shows the typical percentage removal curves as a result of PHEN and PYR adsorption from aqueous solution. With increasing shaking time, the removal efficiency increased. The initial removal was rapid as shown in the rate curve, followed by a relatively slow sorption process, and finally equilibrium was attained. Furthermore, it can be noted that the sorption rates were fast and more than 60% of total sorption occurred within the first 60 min for PHEN and PYR, while a relatively slow adsorption phase was apparent after 600 min for pyrene and 240 min for phenanthrene, respectively.

This trend in adsorption is as a result of availability of adsorption or binding sites on the surface of the adsorbent during initial contact, however, the surface active sites get occupied as the adsorption proceeds thus decreasing the sorption rate due to adsorption to less accessible embedded sites. Fast adsorption is an interesting property of an adsorbent which increases its potential for vast applications (Sepehr *et al.* 2017). The equilibration time was 600 min (15 hours) for PHEN and 1260 min (21 hours) for PYR and extending the shaking time up to 2880 min (48 hours) did not further increase the amount of PAHs adsorbed. This informed the decision to use 24 hours as equilibration time for subsequent experiments.

3.3.3 Effect of initial pH on PAH adsorption

Solution pH plays an important role in the adsorption of hydrophobic organic compounds (HOCs), because it can affect the net charge of the adsorbent and adsorbate, However, the influence of pH is more significant if the compound possesses hydroxyl (-OH) or carboxylic (-COOH) groups because they may easily deprotonate under variable pH conditions. Although such groups are not present in PAHs, they are present in GW (Figure S1). Therefore, the effect of pH

on the adsorption of PHEN and PYR on GW was investigated in the pH range of 2–12 due to the fact that the pH of different surface and waste water can differ.

It can be clearly seen that the removal efficiency of PHEN and PYR is not significantly influenced by varying pH conditions with a standard deviation of 0.46% for PHEN and 0.08% for PYR. It has been reported in literature that pH has no influence on the adsorption of phenanthrene on active silica gel while others have reported that sorption of phenanthrene on kaolinite, quartz, and goethite were affected by solution pH (Huang *et al.* 1996). The results obtained in this study revealed that the optimum pH conditions for the removal of PHEN and PYR were pH below 7. A weak electrostatic repulsion cannot be ruled out between the electron-rich π systems of PHEN and PYR and the negatively charged surface of the adsorbent at basic pH, causing a decrease in the adsorption which is more noticeable for PHEN (Figure 3). However, the influence of pH on the overall adsorption efficiency of PHEN and PYR onto GW is negligible.

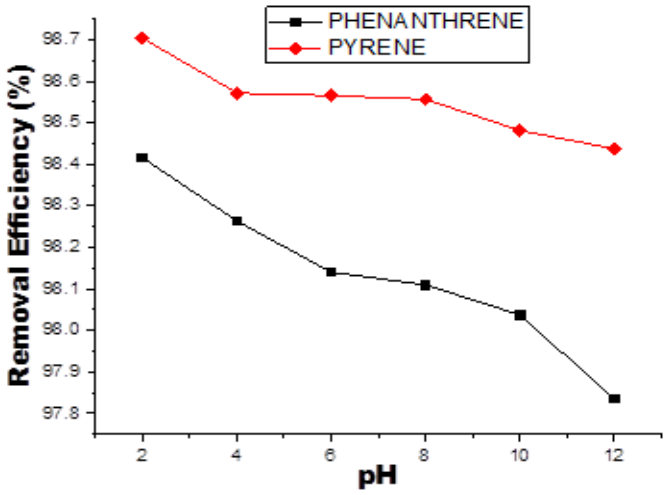

***Figure 3**: Effect of pH on pyrene and phenanthrene adsorption onto graphene wool (Experimental conditions: C_o = 1 mg L^{-1}; dosage = 20 mg per 30 mL, mixing rate = 200 rpm, T = 25 ± 1 °C, contact time: 24 hours).*

3.3.4. Effect of ionic strength/TDS

Total dissolved solids (TDS) and ionic strength play vital roles in water quality (Abdel-Shafy et al., 2016). Several reports suggest that salinity levels may increase or decrease the adsorption capacity of different carbonaceous materials (Xu *et al.* 2012; Zhang *et al.* 2014). Therefore, the effect of ionic strength on the adsorption of PYR and PHEN onto GW was investigated. Experimental data obtained from the study was fit to a linear isotherm equation to evaluate adsorption capacities at varying ionic strength/salinity/TDS according to equation 3:

$$C_s = KdC_e \qquad (3)$$

Where C_s (mg/g) is the amount of PAHs adsorbed, C_e is the equilibrium concentration of PAHs and *Kd* (l/g) is the adsorption capacity.

Figure 4 and Table S3 illustrate that increasing the concentration of NaCl caused a significant increase in the adsorption capacities (*Kd*) of pyrene and phenanthrene with pyrene having the higher adsorption capacity on GW, similar to what was reported in Table 3 for K_f and q_{max} respectively. It has been previously reported that ions such as Ca^{2+}, K^+, Na^+, SO_4^{2-} and Cl^- strongly bind water molecules into hydration shells; thereby reducing the solubility of PAHs in water (Lamichhane *et al.* 2016). Therefore, the cavity volume that accommodates organic solutes, pulls the PAHs molecules onto the hydrophobic surface of GW as a result of increased polarity of the liquid phase by increased salinity levels. The reduction in available water molecules for PAHs dissolution as a result of the strong affinity between the ionic salts and surrounding water molecules is called the "salting out effect"(Lamichhane *et al.* 2016). This phenomenon is responsible for the enhanced adsorption and linearity (considering R^2 and K_d values) which indicates improved partition distribution of the solutes between the solid-liquid interphase.

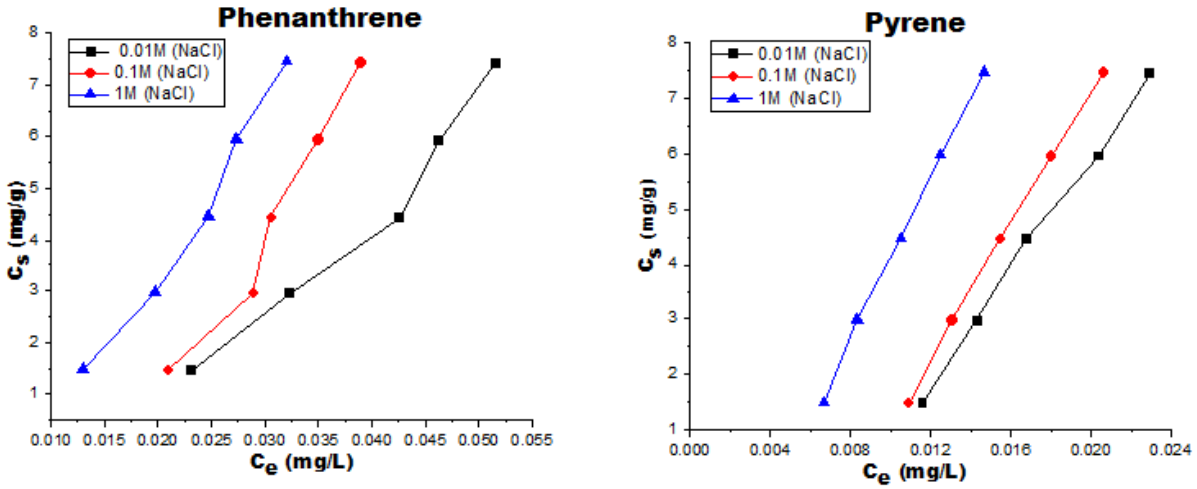

Figure 4: *Effect of ionic strength on adsorption of the selected PAHs from solution (Experimental conditions: NaCl Conc. = 0.01 – 1M; PAH Conc. = 1 - 5 mg L^{-1}; dosage = 20 mg per 30 mL, mixing rate = 200 rpm, T = 25 ± 1 °C).*

3.3.5. Effect of temperature and thermodynamic studies

Temperature plays a significant role in many chemical and physical processes. Some processes are feasible at ambient temperature while others require additional heat energy to raise the temperature within reaction vessels in order to initiate a physical or chemical change. The effect of temperature on the adsorption of phenanthrene (PHEN) and pyrene (PYR) onto graphene wool (GW) was studied at 35, 45 and 55 °C, respectively. The adsorption data was fit to a linear isotherm model (Eq. 3), and it was observed that the equilibrium concentration of the selected PAHs reduced (Figure S4) and adsorption capacity (K_d) increased (Table S4) with increase in temperature. Thermodynamic parameters such as free energy change (ΔG˚), enthalpy (ΔH˚) and entropy (ΔS˚) were calculated using the Van't Hoff equations (Eqs. 4 and 5) derived from Vant't Hoff plots (Figure S5), in order to elucidate the nature of adsorption of PHEN and PYR onto GW as a function of temperature (Yakout & Daifullah 2013).

$$\ln K_d = \frac{\Delta S^\circ}{R} - \frac{\Delta H^\circ}{RT} \quad (4)$$

$$\Delta G^\circ = \Delta H^\circ - T\Delta S^\circ \quad (5)$$

where ΔG is the change in the Gibbs free energy (cal/mol); ΔH is the change in enthalpy (cal/mol), and ΔS is the change in entropy (cal/mol.deg), R = gas constant (1.98 cal/mol K), T = thermodynamic temperature (K) and K_d is adsorption capacity determined from the linear isotherm model.

The thermodynamic parameters calculated using Eqs. (4) and (5) are listed in Table 3. The calculated ΔH° of the PHEN-GW and PYR-GW system is ~12 and ~28 kcal/mole respectively. The positive values of ΔH° and ΔS° indicate that the adsorption process is endothermic with an increase in the randomness between the solid-solution interface as temperature increased (Ahmed & Gasser 2012). The negative value of ΔG indicates spontaneity of the adsorption process and as the temperature increased, the free energy became more negative indicating that the adsorption of PHEN and PYR became more favorable at higher temperature (Table S4 and Figure S4).

The experimental results reported in this work are in agreement with that reported for the adsorption of naphthalene on GO/FeO•Fe_2O_3 and MWCNTs/FeO•Fe_2O_3 (Yang *et al.* 2013). Similarly, results reported for adsorption of 1-naphthol onto sulfonated graphene and 1-naphthylamine onto MWCNTs/iron oxides/β-cyclodextrin reveals similar trends, as both reports indicate that the values of ΔH° and ΔS° are both positive and ΔG° is negative (Zhao *et al.* 2011). However, it is worthy to note that the ΔH° (enthalpy of adsorption) values found in this study are far higher than those reported in literature, in agreement with what was predicted by the Temkin (b_T) and D-R (E) models (Table 2), suggesting the involvement of strong binding energy between GW-PHEN and GW-PYR.

Table 3: Thermodynamic parameters for adsorption of phenanthrene (PHEN) and pyrene (PYR) onto graphene wool (GW)

Temperature (K)	**PHEN**			**PYR**		
	ΔG° (cal/mol)	**ΔH°** (cal/mol)	**ΔS°** (cal/mol.K)	**ΔG°** (cal/mol)	**ΔH°** (cal/mol)	**ΔS°** (cal/mol.K)
308	-2752.78			-6810.76		
318	-3226.58	11,865.7	47.46	-7941.66	28,020.9	113.09
328	-3701.18			-9072.56		

3.4. Desorption isotherms and hysteresis

Desorption studies aid in predicting the release potential and risk of environmental contamination associated with adsorbed organic pollutants. Therefore, evaluating the sorbed fraction that can return to solution by reaching a new equilibrium is expedient. The $K_{f.des}$ and $1/N_{des}$ values which represent the desorption capacity and desorption intensity respectively for GW-PHEN and GW-PYR interactions were obtained by fitting the desorption experimental data to Freundlich isotherms (Cornelissen *et al.* 2005). It is evident from the information presented in Table 4, that the calculated *H* values for both sorbates were greater than zero ($1/N_{ads} > > > 1/N_{des}$), which suggests that sorption–desorption hysteresis occurred (Ololade *et al.* 2018). The calculated hysteresis index was greater in GW-PYR with lesser desorption capacity ($K_{f.des}$) and intensity ($1/N_{des}$) than GW-PHEN, revealing that irreversible entrapment and/or slow rate of desorption of sorbed molecules was more in the heavier PAH compound, possessing a higher binding strength than PHEN (Table 2).

Irreversible pore deformation of adsorbent and hydrophobicity of chemicals has been reported as possible reasons for hysteretic behavior in sorption processes, which may be due to sorbate-induced alteration of the sorbent from its native thermodynamic state via build-up in unrelaxed free volume (Lu & Pignatello 2002). The pore-deformation mechanism has been hypothesized as the main cause of the irreversible sorption of organic compounds sorbed onto carbonaceous materials and several articles have been published in support of this postulate (Nguyen *et al*. 2004).

Table 4: Sorption-desorption parameters and hysteresis index (H) derived from Freundlich isotherm model

Sorbates	**Freundlich Isotherm**				
	$K_{f.des}$	$1/N_{ads}$	$1/N_{des}$	R^2	*H
Phenanthrene	6.89	1.6082	1.4707	0.9750	1.0935
Pyrene	2.55	1.0347	0.5747	0.9147	1.8004

*H: Sorption–desorption hysteresis index, $H=N_{ads}/N_{des}$

3.5. Regeneration experiment

Graphene wool (GW) was regenerated with n-hexane (99.9% purity) by solid phase solvent extraction and reused in eight successive cycles of adsorption experiments. The adsorption efficiency of the GW for PHEN and PYR in the adsorption–regeneration cycles are shown in Figure 5. This regeneration and reusability experiment revealed that GW can potentially be used for the remediation of water contaminated with PAHs for at least eight cycles without significant loss in removal efficiency. The removal efficiency recorded after subsequent regeneration

processes showed that solid-phase extraction at ambient temperature and thermal regeneration at 70ºC was sufficient for the regeneration of GW.

The decision to use hexane was due to its suitable polarity, volatility, easy of recovery and disposal; and because it is relatively environmentally safe. Furthermore, it works very well for GC-MS applications (Berset *et al.* 1999), which is useful for analytical verification of removal efficiencies. It is equally noteworthy that only about 10% weight loss of the GW due to experimental artifacts was recorded over the eight adsorption–regeneration cycles, suggesting that graphene wool is very stable and robust and can withstand a considerable amount of physical stress associated with the regeneration process.

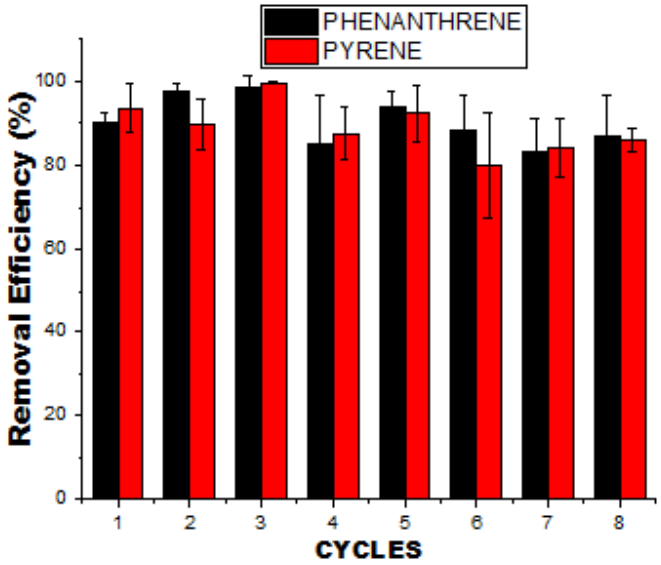

Figure 5*: Removal efficiency of GW after regeneration (Experimental conditions: 25 °C; GW: 20 mg; PAH Conc.: 300 - 800 ng* L^{-1}*, Hexane vol.: 10 mL., n=3).*

3.6. Comparison with previous studies

Table 5 reveals that GW competes favourably with adsorbents that have been reported in literature for the removal phenanthrene (PHEN) and/or pyrene (PYR) as a removal efficiency > 99% was achieved in this study. The maximum adsorption capacity deduced from the Langmuir

isotherm model (q_{max}) and PHEN removal efficiency by GW is higher than that for graphene coated materials (GCMs) and activated carbon (Yang *et al.* 2015; Liu *et al.* 2016). The removal efficiency and adsorption capacity of GW for PYR sorption was found to be higher than that of coke, iron oxide nanoparticles (IONPs), powdered mesoporous organosilica (PMO), biochar, powdered activated carbon, leonardite and graphene oxide (Table 5). The higher adsorption capacity observed for graphene nano-shells (GNS) and activated carbon functionalized with titanate nanotubes (TNT@AC), is likely due to the larger surface area (471.6 m^2/g for TNT@AC, 392 m^2/g for GNS as compared to 279 m^2/g for GW) and hydrophobicity which promotes higher adsorption capacity than the GW used in our study. However, the role of certain experimental variables such as ionic strength and temperature, which has environmental significance with respect to removal of organic pollutants in aqueous medium, were not reported for TNT@AC and GNS (Wang *et al.* 2014; Liu *et al.* 2016). This makes it difficult to ascertain the efficiency of the adsorbents at variable process conditions, whilst these variables were comprehensively evaluated for GW in this study.

The choice of adsorbent for water treatment applications depends on several factors such as efficiency, non-toxicity, availability of material, flexibility, reusability etc. Graphene wool shows great potential for water treatment applications considering that it has a removal efficiency >99%. GW has a very high volume to mass ratio (low density) and is highly porous which makes it a suitable packing material and polishing tool in water treatment applications, because it allows for easy flow of water.

Table 5: Comparison of different materials used for removal of phenanthrene (PHEN) and pyrene (PYR) from aqueous solutions

Adsorbent	**Dosage ($g\ L^{-1}$)**	**Contact Time**	**Removal Efficiency (%)**	**Adsorption Capacity (mg/g)**	**Reference**
Iron oxide nanoparticles (IONPs)	0.09	2.5 hours	98	2.8 (PYR)	(Hassan *et al.* 2018)
Coke derived from porous carbon	1.00	7 hours	99	6.2 (PHEN) 5.0 (PYR)	(Yuan *et al.* 2010)
Wood char	0.005	9 days	≥ 60	-	(Wang *et al.* 2006)
Leonardite (immature coal)	1.00	24 hours	95 (PYR)	-	(Zeledón-Toruño *et al.* 2007)
Wood ash obtained at 800ºC	10	24 hours	100 (PYR)	-	(Pérez-Gregorio *et al.* 2010)
Biochar obtained at 800ºC	2	-	>95 (PYR & PHEN)	-	(Li *et al.* 2014)
Powdered activated carbon (anthracite and coconut shell based)	1.25	30 days	98 (PYR)	-	(Amstaetter *et al.* 2012)
Periodic mesoporous organosilica (PMO)	1.00	24 hours	70	2.6 (PYR)	(Vidal *et al.* 2011)
Activated Carbon	0.5	10 hours	74.9	1.3 (PHEN)	(Liu *et al.* 2016)
Composite of Activated carbon and titanate nanotubes (TNTs@AC)	0.5	3 hours	96.8	12.1 (PHEN)	(Liu *et al.* 2016)
Graphene nanosheets	0.5	90 hours	-	116 (PHEN) 123 (PYR)	(Wang *et al.* 2014)
Graphene oxide	0.5	90 hours	-	5.9 (PHEN) 6.12 (PYR)	(Wang *et al.* 2014)
Graphene coated materials (GCMs)	0.5	36 hours	80	1.74 (PHEN)	(Yang *et al.* 2015)
Graphene wool	*0.67*	*24 hours*	*98.5 - 99.9*	*5 (PHEN)* *20 (PYR)*	*This work*

4.0. Conclusion

These results are of great importance for potential environmental and industrial applications of graphene wool (GW) for the removal of aromatic compounds from large volumes of aqueous solutions. Thermodynamic, kinetic, and isotherm studies showed that the adsorption process of pyrene and phenanthrene onto graphene wool is endothermic and spontaneous in nature. A detailed analysis of isotherm, kinetic and thermodynamic parameters validates the occurrence of strong interaction between GW and the selected PAHs, indicating chemisorption. The q_{max} of GW for PHEN and PYR obtained from the Langmuir isotherms was 5 and 20 mg g^{-1} respectively, which was among the highest values for PHEN and PYR adsorption reported in literature. The isotherm and kinetic data fit well to Sips model and second order kinetic models and PAH concentration played a significant role in determining which isotherm model best fit experimental data. The dominant causes of the sorbate-sorbent affinities are π-π interactions between GW and the conjugated benzene rings of the selected PAHs, together with other complementary sorption mechanisms such as pore filling and hydrophobic effects.

The result of the effect of ionic strength on PHEN and PYR sorption onto GW indicates that the salting-out effect was likely to overcome the influence of competitive sorption, resulting in higher adsorption capacities and removal efficiencies at higher TDS/salinity levels. The optimum pH for the efficient adsorption of the selected PAHs onto GW was determined to be acidic. Furthermore, the experimental results revealed that spent GW can be regenerated and re-utilized via facile solvent extraction and thermal regeneration procedures. Thus, both fresh and regenerated GW adsorbents are economically viable for adsorption of organic pollutants, specifically PAHs.

This comprehensive study revealed that the removal efficiency of PAHs from artificial contaminated water is 98.5 and 99.9 % for pyrene and phenanthrene, respectively, under optimum

process conditions and adsorption increased with increase in the selected PAH concentration. This suggests that removal of PAHs from contaminated or polluted water can be successfully achieved using GW and that this material may be employed in water treatment plants (WTPs) as a polishing tool.

Acknowledgements

Authors acknowledge the University of Pretoria Commonwealth Doctoral Scholarship funding (AA) and the Departments of Chemistry and Physics at the University of Pretoria, especially Prof. Ncholu Manyala, Dr. Liezel Van der Merwe and Genna-Leigh Schoonraad for assistance.

Conflict of interest

The authors declare that there is no conflict of interest regarding the publication of this article.

References

Abdel-Shafy H. I. and Kamel A. H. (2016). Groundwater in Egypt issue: resources, location, amount, contamination, protection, renewal, future overview. *Egyptian Journal of Chemistry* 59, 321-62.

Ahmed I. M. and Gasser M. S. (2012). Adsorption study of anionic reactive dye from aqueous solution to Mg-Fe-CO_3 layered double hydroxide (LDH). *Applied Surface Science* 259, 650-6.

Allen S. J., Mckay G. and Porter J. F. (2004). Adsorption isotherm models for basic dye adsorption by peat in single and binary component systems. *Journal of Colloid and Interface Science* (2), 322–33.

Amstaetter K., Eek E. and Cornelissen G. (2012). Sorption of PAHs and PCBs to activated carbon: Coal versus biomass-based quality. *Chemosphere* 87(5), 573-8.

Berset J. D., Ejem M., Holzer R. and Lischer P. (1999). Comparison of different drying, extraction and detection techniques for the determination of priority polycyclic aromatic hydrocarbons in background contaminated soil samples. *Analytica Chimica Acta.* 383(2), 263–75.

Cai S.-S., Syage J. A., Hanold K. A. and Balogh M. P. (2009). UltraPerformance liquid chromatography−atmospheric pressure photoionization-tandem mass spectrometry for high-sensitivity and high-throughput analysis of U.S. Environmental Protection Agency 16 priority pollutants polynuclear aromatic hydrocarbons. *Analytical* Chemistry 81(6), 2123-8.

Chen J., Chen W. and Zhu D. (2008). Adsorption of Nonionic Aromatic Compounds to Single-Walled Carbon Nanotubes: Effects of Aqueous Solution Chemistry. *Environmental Science and Technology* 42(19), 7225-30.

Cornelissen G., Gustafsson Ö., Bucheli T. D., Jonker M. T. O., Koelmans A. A. and van Noort P. C. M. (2005). Extensive sorption of organic compounds to black carbon, coal, and kerogen in sediments and soils: mechanisms and consequences for distribution, bioaccumulation, and biodegradation. *Environmental Science and Technology* 39(18), 6881-95.

Hassan S. S. M., Abdel-Shafy H. I. and Mansour M. S. M. (2018). Removal of pyrene and benzo(a)pyrene micropollutant from water via adsorption by green synthesized iron oxide nanoparticles. Advances in Natural Sciences: *Nanoscience and Nanotechnology* 9(1), 015006.

Huang W., Schlautman M. A. and Weber W. J. (1996). A distributed reactivity model for sorption by soils and sediments: the influence of near-surface characteristics in mineral domains. *Environmental Science and Technology* 30(10), 2993-3000.

IARC, International Agency for Research on Cancer (2010). IARC monographs on the evaluation of carcinogenic risks to humans. *(Lyon: World Health Organization)* 92, 1–853.

Khan E., Khaodhir S. and Rotwiron P. (2007). Polycyclic aromatic hydrocarbon removal from water by natural fiber sorption. *Water Environment Research* 79(8), 901-11.

Lamichhane S., Bal Krishna K. C. and Sarukkalige R. (2016). Polycyclic aromatic hydrocarbons (PAHs) removal by sorption: a review. *Chemosphere* 148, 336-53.

Li H., Qu R., Li C., Guo W., Han X., He F., Ma Y. and Xing B. (2014). Selective removal of polycyclic aromatic hydrocarbons (PAHs) from soil washing effluents using biochars produced at different pyrolytic temperatures. *Bioresource Technology* 163, 193-8.

Liu W., Cai Z., Zhao X., Wang T., Li F. and Zhao D. (2016). High-capacity and photoregenerable composite material for efficient adsorption and degradation of phenanthrene in Water. *Environmental Science and Technology* 50(20), 11174-83.

Lu Y. and Pignatello J. J. (2002). Demonstration of the “conditioning effect” in soil organic matter in support of a pore deformation mechanism for sorption hysteresis. *Environmental Science and Technology* 36(21), 4553-61.

Martínez M., Miralles N., Hidalgo S., Fiol N., Villaescusa I. and Poch J. (2006). Removal of lead(II) and cadmium(II) from aqueous solutions using grape stalk waste. *Journal of Hazardous Materials* 133(1), 203-11.

Ndiaye N. M., Ngom B. D., Sylla N. F., Masikhwa T. M., Madito M. J., Momodu D., Ntsoane T. and Manyala N. (2018). Three dimensional vanadium pentoxide/graphene foam composite as

positive electrode for high performance asymmetric electrochemical supercapacitor. *Journal of Colloid and Interface Science* 532, 395-406.

Nguyen T. H., Sabbah I. and Ball W. P. (2004). Sorption nonlinearity for organic contaminants with diesel soot: method development and isotherm interpretation. *Environmental Science and Technology* 38(13), 3595-603.

Ololade I. A., Adeola A. O., Oladoja N. A., Ololade O. O., Nwaolisa S. U., Alabi A. B. and Ogungbe I. V. (2018). In-situ modification of soil organic matter towards adsorption and desorption of phenol and its chlorinated derivatives. *Journal of Environmental Chemical Engineering* 6(2), 3485-94.

Pérez-Gregorio M. R., García-Falcón M. S., Martínez-Carballo E. and Simal-Gándara J. (2010). Removal of polycyclic aromatic hydrocarbons from organic solvents by ashes wastes. *Journal of Hazardous Materials* 178(1), 273-81.

Rahman M. S. and Islam M. R. (2009). Effects of pH on isotherms modeling for Cu(II) ions adsorption using maple wood sawdust. *Chemical Engineering Journal* 149, 273–80.

Schoonraad G.-L., Madito M. J., Manyala N. and Forbes P. (2020). Synthesis and optimisation of a novel graphene wool material by atmospheric pressure chemical vapour deposition. *Journal of Materials Science* 55, 545-64.

Sears G. W. (1956). Determination of specific surface area of colloidal silica by titration with sodium hydroxide. *Analytical Chemistry* 28(12), 1981-3.

Sepehr M. N., Al-Musawi T. J., Ghahramani E., Kazemian H. and Zarrabi M. (2017). Adsorption performance of magnesium/aluminum layered double hydroxide nanoparticles for metronidazole from aqueous solution. *Arabian Journal of Chemistry* 10(5), 611-23.

Stoller M. D., Park S., Zhu Y., An J. and Ruoff R. S. (2008). Graphene-based ultracapacitors. Nano Letters 8(10), 3498-502.

Torabian A., Kazemian H., Seifi L., Bidhendi G. N., Azimi A. A. and Ghadiri S. K. (2010). Removal of petroleum aromatic hydrocarbons by surfactant-modified natural zeolite: the effect of surfactant. *CLEAN – Soil, Air, Water* 38(1), 77-83.

Ukalska-Jaruga A., Smreczak B. and Klimkowicz-Pawlas A. (2019). Soil organic matter composition as a factor affecting the accumulation of polycyclic aromatic hydrocarbons. *Journal of Soils and Sediments* 19(4), 1890-900.

Vidal C. B., Barros A. L., Moura C. P., de Lima A. C. A., Dias F. S., Vasconcellos L. C. G., Fechine P. B. A. and Nascimento R. F. (2011). Adsorption of polycyclic aromatic hydrocarbons from aqueous solutions by modified periodic mesoporous organosilica. *Journal of Colloid and Interface Science* 357(2), 466-73.

Wang J., Chen Z. and Chen B. (2014). Adsorption of polycyclic aromatic hydrocarbons by graphene and graphene oxide nanosheets. *Environmental Science and Technology* 48(9), 4817-25.

Wang X., Sato T. and Xing B. (2006). Competitive sorption of pyrene on wood chars. *Environmental Science and Technology* 40(10), 3267-72.

Xu J., Wang L. and Zhu Y. (2012). Decontamination of bisphenol-A from aqueous solution by graphene adsorption. *Langmuir* 28(22), 8418-25.

Yakout S. M. and Daifullah A. A. M. (2013). Removal of selected polycyclic aromatic hydrocarbons from aqueous solution onto various adsorbent materials. *Desalination and Water Treatment* 51(34-36), 6711-8.

Yang K., Chen B. and Zhu L. (2015). Graphene-coated materials using silica particles as a framework for highly efficient removal of aromatic pollutants in water. *Scientific Reports* 5, 11641.

Yang K. and Xing B. (2007). Desorption of polycyclic aromatic hydrocarbons from carbon nanomaterials in water. *Environmental Pollution* 145(2), 529-37.

Yang X., Li, J., Ren X., Huang Y. and Wang X. (2013). Adsorption of naphthalene and its derivatives on magnetic graphene composites and the mechanism investigation. *Colloid Surface A*. 422, 118– 25.

Yu F., Ma J. and Bi D. (2015). Enhanced adsorptive removal of selected pharmaceutical antibiotics from aqueous solution by activated graphene. *Environmental Science and Pollution Research* 22(6), 4715-24.

Yuan M., Tong S., Zhao S. and Jia C. Q. (2010). Adsorption of polycyclic aromatic hydrocarbons from water using petroleum coke-derived porous carbon. *Journal of Hazardous Materials* 181(1-3), 1115-20.

Zeledón-Toruño Z. C., Lao-Luque C., de las Heras F. X. C. and Sole-Sardans M. (2007). Removal of PAHs from water using an immature coal (leonardite). *Chemosphere* 67(3), 505-12.

Zhang Y.-L., Liu Y.-J., Dai C.-M., Zhou X.-F. and Liu S.-G. (2014). Adsorption of clofibric acid from aqueous solution by graphene oxide and the effect of environmental factors. *Water, Air, & Soil Pollution* 225(8), 2064-74.

Zhao G. X., Li J. X. and Wang X. K. (2011). Kinetic and thermodynamic study of 1-naphthol adsorption from aqueous solution to sulfonated graphene nanosheets. *Chemical Engineering Journal* 173, 185–90.